

The University
of Manchester

MANCHESTER
1824

**Double Beta Decay Studies for ^{150}Nd
at the Neutrino Majorana Observatory
(NEMO3) Experiment**

Nasim Fatemi-Ghomi

May 2006

Particle Physics Group
School of Physics and Astronomy

A first year PhD report

Contents

1	Introduction	8
2	Neutrino Theory	9
2.1	The Standard Model	9
2.2	Neutrino Mass in the Extension to the Standard Model	11
2.3	Double Beta Decay	11
2.3.1	Neutrinoless Double Beta Decay	13
2.3.2	Further Theories for Neutrinoless Double Beta Decay	14
3	The NEMO3 Experiment	16
3.1	General Description of the Detector	16
3.2	Source foils	18
3.3	Sources of background to ^{150}Nd	20
4	Analysis	22
4.1	Double beta decay event selection	22
4.2	Background to Double Beta Decay Estimation	28
4.2.1	^{207}Bi decay to ^{207}Pb	28
4.2.2	Other Sources of Background	32
4.3	Preliminary measurement of the half-life of $^{150}\text{Nd} \rightarrow 2\nu\beta\beta$	33

List of Figures

2.1	A schematic diagram of the energy requirements for double beta decay	12
2.2	Diagram for a) normal double beta decay and b) neutrinoless double beta decay.	13
2.3	Neutrinoless double beta decay with Majoron emission.	15
2.4	Total energy sum of the two electrons emitted from ^{100}Mo (an isotope of molybdenum), for $2\nu\beta\beta$ decay (blue), $0\nu\beta\beta$ (red) and one of the possible hypotheses of Majoron emission (green)[6]	15
3.1	Cutaway view of the NEMO3 detector	17
3.2	The source distribution in the 20 sectors of NEMO3.	18
3.3	Decay chain of ^{207}Bi	21
4.1	Energy distribution of the lowest energy electron. The data is shown with error bars. The simulated background normalized by their activities, are shown with different colors. The simulated $2\nu\beta\beta$ is shown with red. The data is compared with total MC (sum of the simulated background and simulated $2\nu\beta\beta$).	24
4.2	The distribution of the distance between the origins of the tracks a) in the $x - y$ plane b) in the z direction.	25
4.3	The distribution of the probabilities of the two examined a) internal and b) external time of flight hypotheses.	26
4.4	a) Sum of the energy of electrons and b) cosine of angle between electron tracks for events passed the event selection criteria. The $2\nu\beta\beta$ MC events are scaled with the number of data events.	27

4.5	a) Distribution of the energy of the electron and b) Distribution of the energy of the γ -ray for $e\gamma$ channel. The number of simulated $2\nu\beta\beta$ events is scaled with the number of data minus background events. The data does not have a good fit with simulated events. Cuts are made in the energy region $0.8 < E_e < 1.1$ and $0.27 < E_\gamma < 0.6$, where the background is small.	30
4.6	a) Distribution of the energy of the electron and b) Distribution of the energy of the γ -ray for $e\gamma$ channel after applying $0.8 < E_e < 1.1$ and $0.27 < E_\gamma < 0.6$ energy conditions.	31
4.7	a)The sum of the energy of two electrons. b)The energy distribution of the lower energy electron. c)The cosine of the angle between two electrons. The $2\nu\beta\beta$ MC events are scaled with the number of data events minus the number of total internal background events.	34

List of Tables

2.1	The three generations of fermions in the Standard Model, their electric charge and mass[1].	10
2.2	The gauge bosons of the Standard Model and their masses [1]. . .	10
3.1	Isotopes used for double beta decay studies.	19
4.1	Contaminants of ^{150}Nd and a preliminary measurement of their activities in mBq/kg [7] done with the Ge detector.	32
4.2	The table of results	35

Abstract

A study of two-neutrino double beta decay for ^{150}Nd source foil with the NEMO3 detector is presented. The background to this decay is estimated with the help of the activities of the contaminants of ^{150}Nd . The ^{207}Bi background has been separately determined using the $e - \gamma$ process. The preliminary measured half-life of this process is

$$T_{1/2}^{2\nu\beta\beta} = (8.02 \pm 0.32 \text{ (stat)} \pm 0.41 \text{ (syst)}) \times 10^{18} \text{ years.}$$

This work continues with improving this result and reducing the systematic uncertainties. Finally, a limit on the half-life of neutrinoless double beta decay will be set.

Chapter 1

Introduction

One of the fundamental challenges in particle physics is to investigate about the nature of neutrinos. The primary objective of the NEMO3 experiment is to search for neutrinoless double beta decay. Observation of neutrinoless double beta decay, $0\nu\beta\beta$, would prove that neutrinos are their own antiparticles and therefore Majorana particles. Experimental signature of this process is the observation of the two electrons, for which the total energy sum is exactly the nuclear transition energy, and physical observable that has to be measured is the half-life of this process.

This report starts with a brief theoretical review of the double beta decay process in Chapter 2. Chapter 3 gives a detailed description of the NEMO3 experiment. Chapter 4 describes the work done towards a measurement of the half-life of $2\nu\beta\beta$ decay for ^{150}Nd isotope and to background studies for this channel.

Chapter 2

Neutrino Theory

2.1 The Standard Model

The Standard Model was created to describe the observed interactions of particles. In the Standard Model there are two general classes of fundamental particles: *Fermions*, which have spin $\frac{1}{2}$, and *gauge bosons*, which have spin 1. The twelve fundamental types of fermions are subdivided into two groups, leptons and quarks. There are three generation of leptons and quarks each, which have similar properties but different masses. The properties of fermions are given in Table 2.1. The interactions of particles in the Standard Model are mediated by the exchange of a gauge boson. The gauge bosons of the electroweak and of the strong interaction are given in Table 2.2.

	fermions	charge	mass
leptons	electron (e)	-1	0.51 MeV
	electron-neutrino (ν_e)	0	0
	muon (μ)	-1	105.6 MeV
	muon-neutrino (ν_μ)	0	0
	tau (τ)	-1	1777 MeV
	tau-neutrino (ν_τ)	0	0
quarks	up (u)	+2/3	1.5-4 MeV
	down (d)	-1/3	4-8 MeV
	charm (c)	+2/3	1.15-1.35 GeV
	strange (s)	-1/3	80-130 MeV
	top (t)	+2/3	174 ± 5.1 GeV
	bottom (b)	-1/3	4.1-4.4 GeV

Table 2.1: The three generations of fermions in the Standard Model, their electric charge and mass[1].

gauge bosons	interaction	mass (GeV)
γ (photon)	electromagnetic	0
Z boson	weak	91.188 ± 0.002
W^\pm boson	weak	80.425 ± 0.038
g (gluon)	strong	0

Table 2.2: The gauge bosons of the Standard Model and their masses [1].

2.2 Neutrino Mass in the Extension to the Standard Model

The Standard Model gives fermions mass through the *Higgs mechanism* [2]. The Higgs field has a non-zero expectation value and particles acquire mass through coupling to this field. The value of mass depends on the strength of the coupling.

Neutrinos are left-handed and massless in the Standard Model. To generate mass for the neutrino we must have an extension to the Standard Model. There are several additions to the model which could generate mass for the neutrinos. These models suggest two possible types of massive neutrinos. Generally the neutrino may be either a *Dirac* particle which means whilst the neutrino and antineutrino are distinct, only left-handed neutrino can be observed. Alternatively the neutrino may be a *Majorana* particle (left or right-handed). In this case, the neutrino and antineutrino are indistinguishable.

2.3 Double Beta Decay

Beta decay (β^-) is a type of radioactive decay in which a beta particle (an electron) is emitted. In β^- decay, the weak interaction converts a neutron into a proton while emitting an electron and an antineutrino:

$$n \rightarrow p + e^- + \bar{\nu}. \quad (2.1)$$

Double beta decay, $2\nu\beta\beta$ [3], is a nuclear decay process in which two standard beta decay occurs simultaneously with the emission of two electrons and two an-

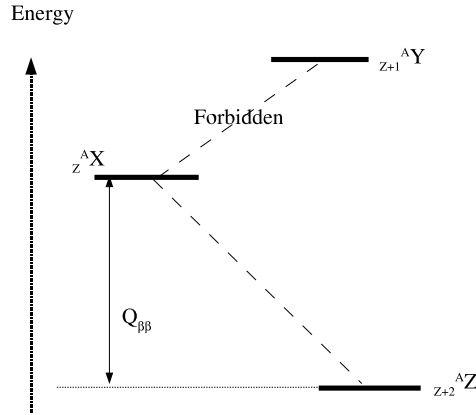


Figure 2.1: A schematic diagram of the energy requirements for double beta decay
 tineutrinos:

$$(A, Z) \rightarrow (A, Z + 2) + 2e^- + 2\bar{\nu}_e, \quad (2.2)$$

where A and Z are the atomic mass and atomic number of the isotope.

Double beta decay occurs when a parent nucleus A_ZX decays to a daughter nucleus $^A_{Z+2}Z$ because the intermediate single beta decay to $^A_{Z+1}Y$ is energetically forbidden. A schematic diagram of the energy requirements for double beta decay is shown in Figure 2.1. Double beta decay is the rarest known kind of radioactive decay, and it is observed in only 35 isotopes. As it is shown in Figure 2.2. a, double beta decay involves two weak interactions and so the rate of the process is characterised by its very long lifetime (more than 10^{18} years). The half-life $T_{2\nu}^{1/2}$ of the double beta decay process is expressed by the equation

$$[T_{1/2}^{2\nu}]^{-1} = G^{2\nu}|M^{2\nu}|^2, \quad (2.3)$$

where $G^{2\nu}$ is an analytically calculable phase space integral, and $M^{2\nu}$ is the Nuclear Matrix Element (NME) for double beta decay which can be calculated ap-

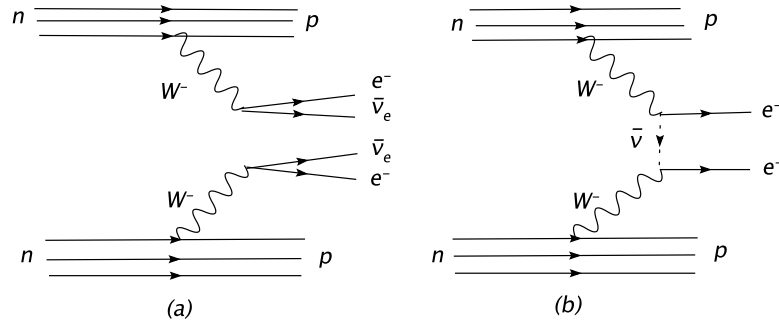


Figure 2.2: Diagram for a) normal double beta decay and b) neutrinoless double beta decay.

proximately and gives the probability of the process. To test the methods used to calculate NMEs, it is important to determine the half-life of $2\nu\beta\beta$ experimentally. The accurate measurement of double beta decay is important, as this forms the irreducible background to the neutrinoless double beta decay signal.

2.3.1 Neutrinoless Double Beta Decay

The neutrinoless double beta decay ($0\nu\beta\beta$) involves a transition of two neutrons into two protons with the emission of two electrons and nothing else (Figure 2.2.b). This process can occur if and only if neutrinos are light Majorana [4] particles. In this case an right-handed antineutrino (=neutrino) emitted at one vertex undergoes a helicity flip and gets absorbed into the other vertex as a left-handed neutrino; therefore no neutrino is observed in the final state. The decay rate scales with the fifth power of the nuclear transition energy $Q_{\beta\beta}$, so it is vital to pick isotopes with high $Q_{\beta\beta}$ to reduce the background from natural radioactive which contributes mainly at low Q values.

The neutrinoless double beta decay process is expected to have a longer half-life

than $2\nu\beta\beta$ because the antineutrino emitted at one vertex must be absorbed at the other one as a neutrino. The half-life of $0\nu\beta\beta$ is connected to the effective neutrino mass ($\langle m_\nu \rangle$) by the relation

$$[T_{1/2}^{0\nu}]^{-1} = G^{0\nu} |M^{0\nu}|^2 |\langle m_\nu \rangle|^2. \quad (2.4)$$

If the neutrinoless double beta decay is not observed, the lower limits on the experimentally measured half-life simultaneously provide upper limits on the effective neutrino mass. Accuracy in calculating the nuclear matrix elements is clearly an important factor in determining $\langle m_\nu \rangle^2$ and in demonstrating the Majorana nature of the neutrino.

2.3.2 Further Theories for Neutrinoless Double Beta Decay

Several theories beyond the Standard Model predict neutrinoless double beta decay. One mechanism which may contribute to $0\nu\beta\beta$ process is the emission of a *Majoron*, M_0 , the Goldstone boson associated with spontaneous symmetry breaking of lepton number. A number of possible decays exist, the simplest of which is neutrinoless double beta decay with light Majorana neutrino exchange and the emission of a single Majoron[5]

$$(A, Z) \rightarrow (A, Z + 2) + 2e^- + M^0, \quad (2.5)$$

as shown in Figure 2.3.

The expression for the half-life of this process is:

$$[T_{1/2}^{0\nu}]^{-1} = G^{0\nu} |M^{0\nu}|^2 |\langle g_{ee} \rangle|^2, \quad (2.6)$$

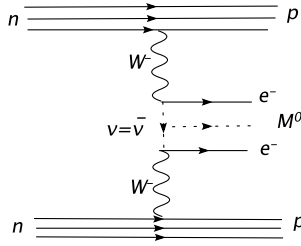


Figure 2.3: Neutrinoless double beta decay with Majoron emission.

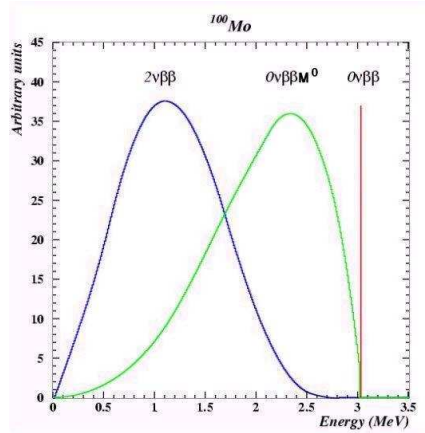


Figure 2.4: Total energy sum of the two electrons emitted from ^{100}Mo (an isotope of molybdenum), for $2\nu\beta\beta$ decay (blue), $0\nu\beta\beta$ (red) and one of the possible hypotheses of Majoron emission (green)[6].

where $M^{0\nu}$ is the appropriate NME and $\langle g_{ee} \rangle$ is the Majoron coupling constant.

In double beta decay experiments such as NEMO3, the total energy of the two emitted electrons is measured. The $0\nu\beta\beta$ decay signal should produce a sharp peak at energy $Q_{\beta\beta}$, whereas the $0\nu\beta\beta M^0$ is expected to have a different energy spectrum from the $2\nu\beta\beta$ decay. Therefore, by measuring the energy spectrum, different types of the $\beta\beta$ process can be reconstructed. Figure 2.4 shows the spectrum of the energy sum of the two electrons emitted from ^{100}Mo , for different types of $\beta\beta$ decays.

Chapter 3

The NEMO3 Experiment

The Neutrino Ettore Majorana Observatory 3 (NEMO3) [7] experiment is running in the Fréjus Underground Laboratory in France. The experiment is searching for evidence of neutrinoless double beta decay in a variety of different isotopes. The NEMO3 aims to measure effective neutrino mass down to a level of a few hundred meV. If no event is observed by the end of its run, a lower limit on $0\nu\beta\beta$ half-life and an upper limit on $\langle m_\nu \rangle$ will be reached.

3.1 General Description of the Detector

The NEMO3 detector shown in Figure 3.1, is cylindrical in design and divided radially into 20 equally large sectors, each of which houses its own source foil. The segmentation permits easy access to source foils of the different isotopes. The source foils are between 30 and 60 mg/cm² thick and 2.5 m in height. They are fixed vertically at a radius of 1.55 m between two concentric cylindrical tracking

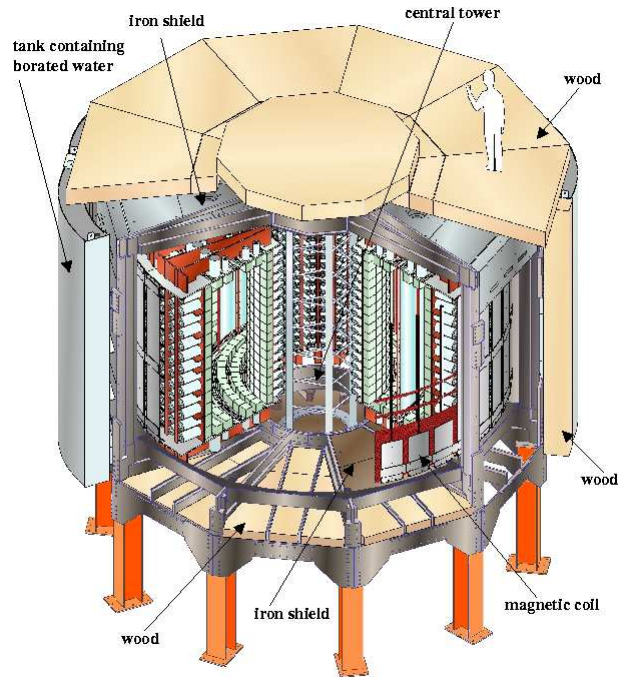


Figure 3.1: Cutaway view of the NEMO3 detector

volumes, composed of 6180 open octagonal drift cells and filled with a gas mixture of helium, ethyl alcohol and argon at 7 mbar above atmospheric pressure. The drift cells are 270 cm long, operating in Geiger mode. The cells run vertically and three-dimensional tracking is accomplished by measuring the arrival time of the signals on the anode wires and the plasma propagations times to the ends of the drift cells. The tracking detector is capable of detecting electrons, positrons and α -particles.

The energy and time of flight of particles are measured by plastic scintillators surrounding the tracking volume. To further enhance the acceptance, the end-caps (the top and bottom of the detector) are also equipped with scintillators in the spaces between the drift cell layers. The calorimeter is made of 1940 large blocks of scintillators coupled to very low radioactivity 3" or 5" photo multiplier

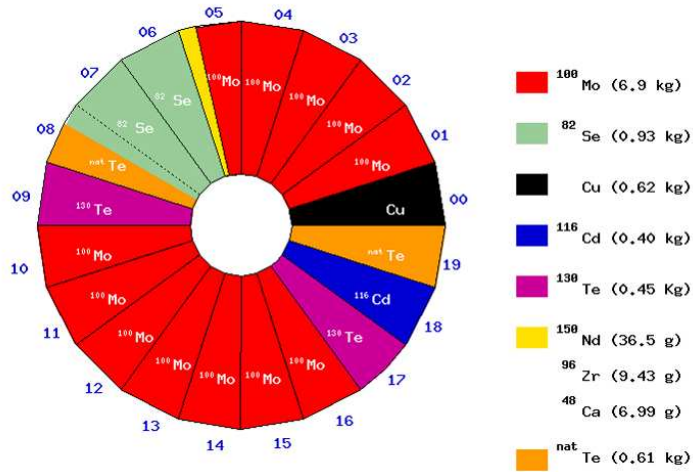


Figure 3.2: The source distribution in the 20 sectors of NEMO3.

tubes (PMTs). The 10 cm thick blocks of scintillator yield a high photon detection efficiency.

3.2 Source foils

The choice of source nuclei for NEMO3 was based on a several factors: the transition energy $Q_{\beta\beta}$, the phase space factors $G^{0\nu}$ and $G^{2\nu}$, the Nuclear Matrix Elements of the transitions for $0\nu\beta\beta$ and $2\nu\beta\beta$ decays ($M^{0\nu}$ and $M^{2\nu}$), the background in the energy region around the $Q_{\beta\beta}$ value, and finally the natural abundance of the isotope. Each sector of the detector contains a segment of source foil made from seven individual strips of mean length 2480 mm and mean width 64 mm. Nine isotopes in various quantities were chosen for NEMO3 and these are placed in the “NEMO3 Camembert” structure displayed in Figure 3.2.

Double beta decay occurs in seven of these isotopes: ¹¹⁶Cd, ⁸²Se, ¹⁰⁰Mo, ⁹⁶Zr, ¹⁵⁰Nd, ⁴⁸Ca and ¹³⁰Te. The $Q_{\beta\beta}$ and the natural abundance of these isotopes are

Transition	$Q_{\beta\beta}$	Abundance (%)
$^{130}\text{Te} \rightarrow ^{130}\text{Xe}$	2528.8 ± 2.1	33.8
$^{116}\text{Cd} \rightarrow ^{116}\text{Sn}$	2804.7 ± 4.2	7.5
$^{82}\text{Se} \rightarrow ^{82}\text{Kr}$	2995.2 ± 3.3	9.2
$^{100}\text{Mo} \rightarrow ^{100}\text{Ru}$	3034.8 ± 6.3	9.6
$^{96}\text{Zr} \rightarrow ^{96}\text{Mo}$	3350.0 ± 3.5	2.8
$^{150}\text{Nd} \rightarrow ^{150}\text{Sm}$	3367.1 ± 4.9	5.6
$^{48}\text{Ca} \rightarrow ^{48}\text{Ti}$	4272.0 ± 4.1	0.187

Table 3.1: Isotopes used for double beta decay studies.

given in Table 3.2. All isotopes are suitable for double beta decay studies, except ^{130}Te which has a low $Q_{\beta\beta}$ and therefore a high radioactive background. The final two isotopes which have a negligible internal background (Cu and $^{\text{nat}}\text{Te}$) are used for measuring external backgrounds in the experiment.

^{150}Nd source

One of the highest $Q_{\beta\beta}$ value isotopes in the detector is ^{150}Nd . The single neodymium composite strip is made of 40.2 g of enriched Nd_2O_3 . This gives a total mass of 37.0 ± 0.1 g ^{150}Nd . The main purpose of this work is to carry out precise studies of background to $2\nu\beta\beta$ and $0\nu\beta\beta$ decays of ^{150}Nd , find the value for the half-life of $2\nu\beta\beta$, search for $0\nu\beta\beta$ and put a lower limit for a $0\nu\beta\beta$ half-life if $0\nu\beta\beta$ is not going to be observed for this isotope.

3.3 Sources of background to ^{150}Nd

The choice of isotopes was partially dictated by their transition energies, with a view of minimising the natural radioactivity with energies in the same region which can produce $\beta\beta$ -mimicking decays. Two main categories of background, internal and external, can affect the results.

Internal backgrounds to $0\nu\beta\beta$ come from contaminants in the source foil, most important of which are the high energy tail of $2\nu\beta\beta$ decay, which cannot be isolated from the $0\nu\beta\beta$ signal, and the natural β -decay chains of ^{214}Bi and ^{208}Tl which are present in the source foil at some level. These isotopes produce decays that mimic $\beta\beta$ events in three ways:

- A β -decay accompanied by an electron from an electron conversion¹ process will give two electrons of sufficient energy from a single vertex.
- Møller scattering of a β -decay electron in the foil. In this case two electrons are produced from a Møller scattered β particle.
- A second electron produced following β -decay emission via a Compton scattered γ -ray.

The equipment used for ^{150}Nd treatment was possibly polluted with a very small amount of ^{207}Bi atoms. Therefore, this isotope is the major contaminant of ^{150}Nd in NEMO3. The ^{207}Bi can undergo an electron capture process (β^+) and decay to the excited state of ^{207}Pb , which itself can become stable by emitting one electron

¹ electron conversion happens when the multipole electric field of the nucleus interact with an orbital electron and eject it from the atom.

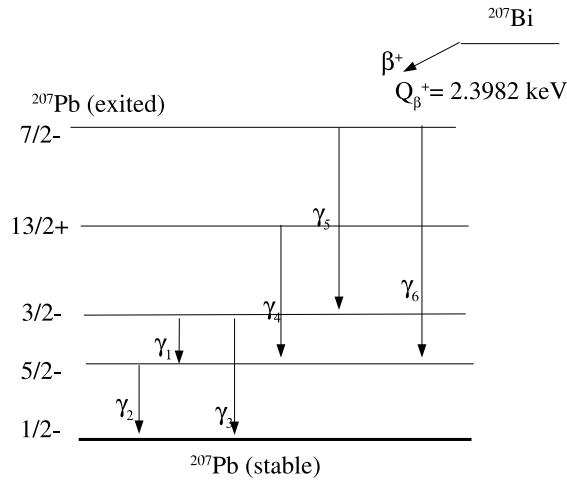


Figure 3.3: Decay chain of ^{207}Bi

and one γ -ray or two electrons from the internal conversion process (Figure 3.3), which can be a source of background to double beta decay.

External background come from sources outside the foil which then interact with the foil to produce a signal. High-energy external γ -ray sources can initiate e^+e^- pair production in the detector. Radioactivity from the PMTs, radon and fast neutrons can also be problem backgrounds. Radon (^{222}Rn) and thoron (^{220}Rn) mainly come from the surrounding rocks and are present in varying concentrations in free air. They can enter the detector and undergo α -decay giving ^{218}Po and ^{216}Po , which have ^{214}Bi and ^{208}Tl as daughter isotope. Since December 2004, when a second running period started, the radon level has been reduced by a factor of ten by introducing a radon-tight tent enclosing the detector, and a radon-trap facility. The data collected in the first running period with high radon contamination are referred to as Phase I data, whereas the data with lower radon contamination are referred to as Phase II data.

Chapter 4

Analysis

This chapter describes the preliminary measurement for half-life of the $2\nu\beta\beta$ of ^{150}Nd . The analysis is performed on data recorded in Phase I of the data collecting time. All events are required to have a vertex between sector values of 5.7371 and 5.8706 (Figure 3.2), corresponding to the ^{150}Nd source foil region.

4.1 Double beta decay event selection

The signature of $2\nu\beta\beta$ is two tracks with negative curvature, associated with two isolated scintillator hits. Tracks must start from layers 1 and 2 of the Geiger cells closest to the foil. This cut reject events with electrons not coming from the foil.

To reduce the background contribution from radon, we reject ^{214}Bi - ^{214}Po events producing two electron tracks accompanied by an α -particle which is identified by the presence of delayed Geiger cell hits. As the range of α -particles from the ^{214}Bi decay in the He gas of the NEMO3 wire chamber is about 25-40 cm, the

distance between the reconstructed vertex and the delayed Geiger cell(s) corresponding to an α -particle, is required to be $|\Delta z| < 30$ cm in vertical direction and $|\Delta r| = |\sqrt{(\Delta x)^2 + (\Delta y)^2}| < 25$ cm in $x - y$ plane. Events are rejected if within this distance there is a single delayed Geiger cell hit with time delay $> 70 \mu\text{s}$ or there are more than two Geiger cell hits with time delay $> 20 \mu\text{s}$ and a time difference between aligned hits $< 2 \mu\text{s}$.

In addition to the pre-selections described above, further selections must be applied. Figures 4.1 to 4.3 show the distribution of each cut variable. In each histogram, the data is shown with error bars. The simulated background events are normalized by the activities found by Ge detector ¹ 4.2.2, and shown with different colours. The $2\nu\beta\beta$ MC simulation (red) is scaled with the total number of radioactive background events subtracted from number of data events. The sum of the $2\nu\beta\beta$ and background MCs (gray) is also shown in the histograms.

The event selection criteria are:

- The energy of both electrons (E_{1e} and E_{2e}) must be larger than 200 keV. Figure 4.1 shows the energy distribution of the lowest energy electron.

- In order to reject the events with tracks not originating from a common vertex the distance between the origins of tracks in the foil is measured.

Events are rejected with:

$$|\Delta r| = |\sqrt{(\Delta x)^2 + (\Delta y)^2}| > 2 \text{ cm in the horizontal } x - y \text{ plane (Figure 4.2a).}$$

$$|\Delta z| > 4 \text{ cm in the vertical } z \text{ direction (Figure 4.2b).}$$

- To reduce the events with tracks coming from outside the foil, the time-of-

¹ The Ge detectors are capable of measuring the radioactivity by γ -ray cascade.

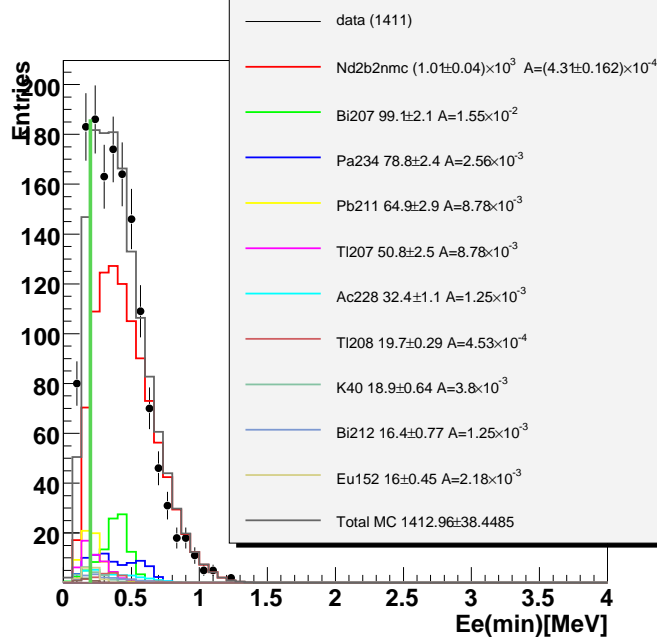


Figure 4.1: Energy distribution of the lowest energy electron. The data is shown with error bars. The simulated background normalized by their activities, are shown with different colours. The simulated $2\nu\beta\beta$ is shown with red. The data is compared with total MC (sum of the simulated background and simulated $2\nu\beta\beta$).

flight (TOF) test is implemented. There are two hypotheses for the origin of the two reconstructed tracks. The first hypothesis is the internal origin of the two electrons, meaning that they were both generated at the same time t_0 at a common point inside the source foil, then they went through the wire chamber and were detected with two distinct scintillators. The second hypothesis is that an external particle entered the tracking volume of the detector through one scintillator, crossed through the source foils and was finally detected by another scintillator. To decide, the most powerful method is a χ^2 -based TOF test. For each two-electron event, the values of χ_{int}^2 and χ_{ext}^2 are calculated and the probabilities of the two examined hypotheses are

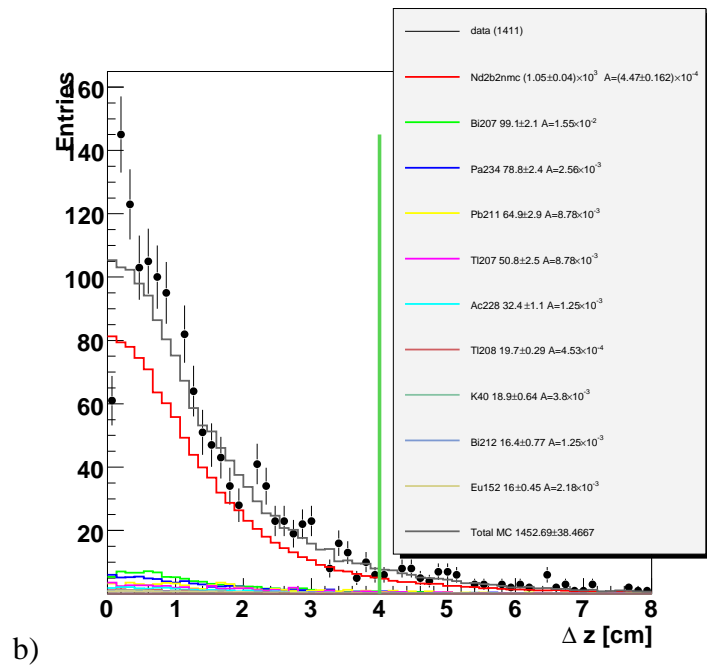
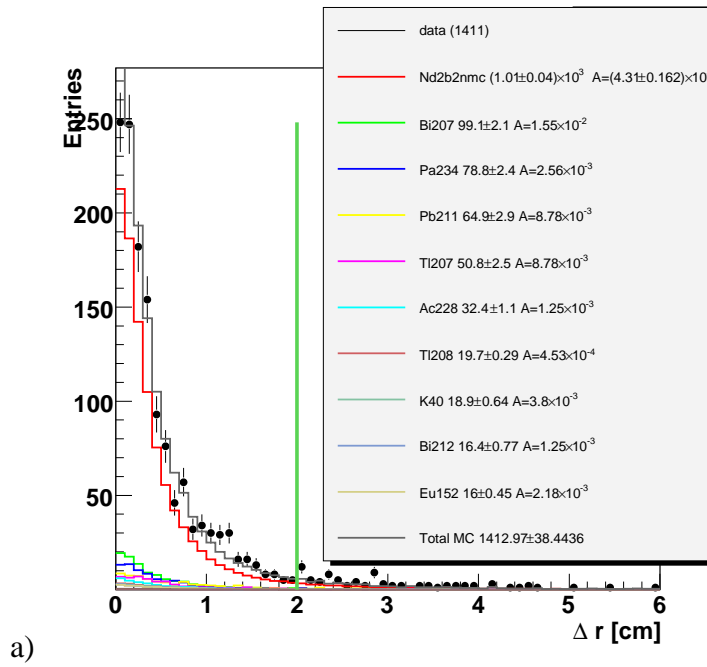


Figure 4.2: The distribution of the distance between the origins of the tracks a) in the $x - y$ plane b) in the z direction.

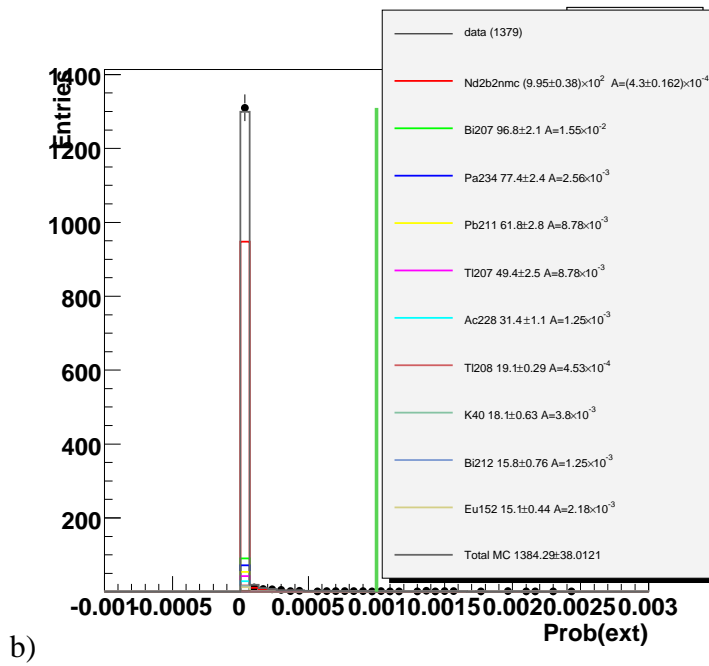
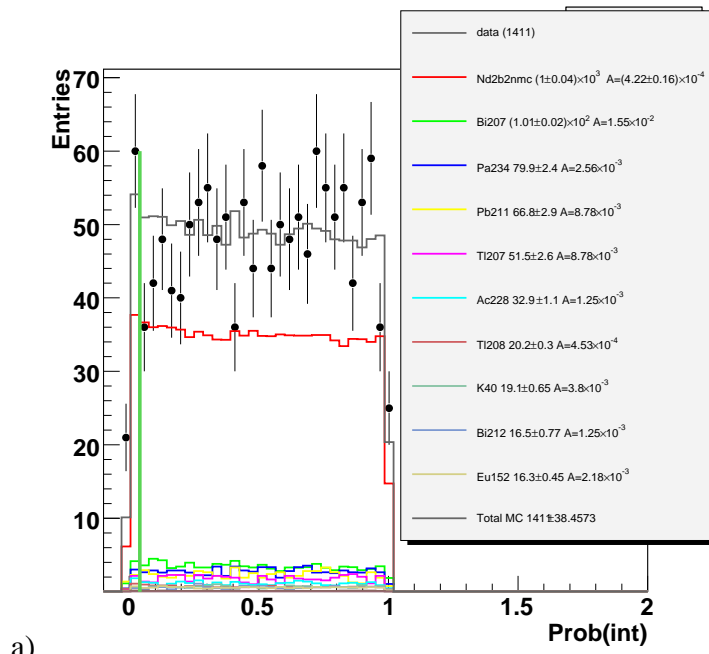


Figure 4.3: The distribution of the probabilities of the two examined a) internal and b) external time of flight hypotheses.

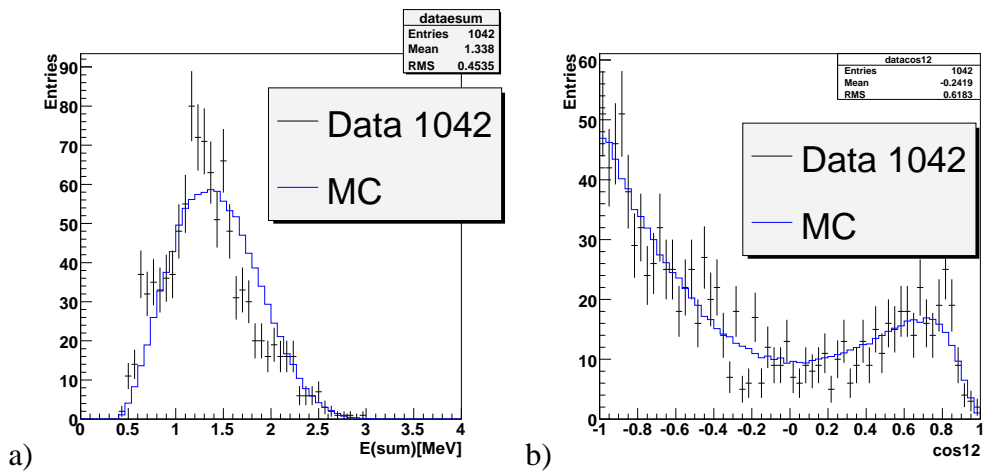


Figure 4.4: a) Sum of the energy of electrons and b) cosine of angle between electron tracks for events passed the event selection criteria. The $2\nu\beta\beta$ MC events are scaled with the number of data events.

deduced (i.e. whether the event is either of the internal origin type, or of the crossing particle type). A good internal two-electron event has to satisfy the following conditions:

The probability of the internal hypothesis has to be greater 4% (Figure 4.3a).

The probability of the external hypothesis has to be less than 1% (Figure 4.3b).

Figure 4.4 shows the energy sum of the two electrons and the cosine of the angle between electron tracks for the events that passed all the event selection conditions. The $2\nu\beta\beta$ MC events are scaled with the number of data events. There is not a good agreement with the MC and data. Therefore, there are some background events left in the selected data events that need to be reduced.

4.2 Background to Double Beta Decay Estimation

Although the event selection criteria described in section 4.1 reject most of the background events, there are some background events left in the data. By measuring the activity for each contaminant and normalizing the MC simulation to the activity found, it will be possible to estimate the internal background with the highest precision.

The activity A , of each isotope is defined by its number of decays per second,

$$A = \frac{(N_{exp} - N_{bgr})}{t \epsilon}, \quad (4.1)$$

where N_{exp} is the number of experimental data events found for the decay channel, N_{bgr} is the number of background events remaining in the data sample, t is the total data taking period and ϵ is the efficiency of the event selection criteria. The number of total background events is found by:

$$N_{bgr} = \sum_i \frac{A_i N_{MC_i} t}{N_{gen_i}}, \quad (4.2)$$

where N_{MC_i} is the number of the MC contaminant events that pass the event selection criteria and N_{gen_i} is the number of generated MC events.

4.2.1 ^{207}Bi decay to ^{207}Pb

As described in Section 3.3 a major source of internal background to $2\nu\beta\beta$ decay is the ^{207}Bi decay to ^{207}Pb . To find the activity of this isotope we look at $^{207}\text{Bi} \rightarrow e\gamma$ channel. The event selection criteria for this channel are as follows:

- Only one negatively charged track associated with an isolated scintillator hit with energy > 200 keV.

- Only one γ cluster with energy > 200 keV.
- Internal TOF hypothesis for $e\gamma$ events $> 1\%$ and external TOF hypothesis $< 1\%$.
- Tracks must start from layer 1 and 2 of the Geiger cells.

Figure 4.5 shows the distribution of the electron and γ -ray energy after applying these event selection criteria. Here, all $e\gamma$ data events are fitted with ^{207}Bi MC. As it can be seen from the histograms, this procedure overestimates ^{207}Bi and does not describe the data well. The reason for this is that the background to ^{207}Bi is underestimated. We therefore look at the energy range $0.8 < E_e < 1.1$ MeV and $0.27 < E_\gamma < 0.6$ MeV, where the estimated background is small and ^{207}Bi dominates over all other background.

The result is shown in Figure 4.6. The efficiency for the $^{207}\text{Bi} \rightarrow e\gamma$ event selection criteria is found by

$$\epsilon = \frac{N_{MC}^{sel}}{N_{MC}^{gen}} = \frac{72208}{10^6} = (0.72 \pm 0.04(\text{sys}))\%, \quad (4.3)$$

where N_{MC}^{sel} is the number of the MC events passed the event selection criteria and N_{MC}^{gen} is the number of generated MC events. The 5% systematic uncertainty on the efficiency comes from the uncertainty on MC simulation [8].

The data taking period is 2.8836×10^7 s. The number of the data events passing the event selection criteria is 3464, the number of estimated background events is 244. Because of the underestimated background, we assume 100% uncertainty on this background. By substituting these values in equation 4.1, the activity is found to be:

$$A = 272 \pm 21 (\text{bgr}) \pm 14 (\text{eff}) \pm 5 (\text{stat}) \text{ mBq/kg}. \quad (4.4)$$

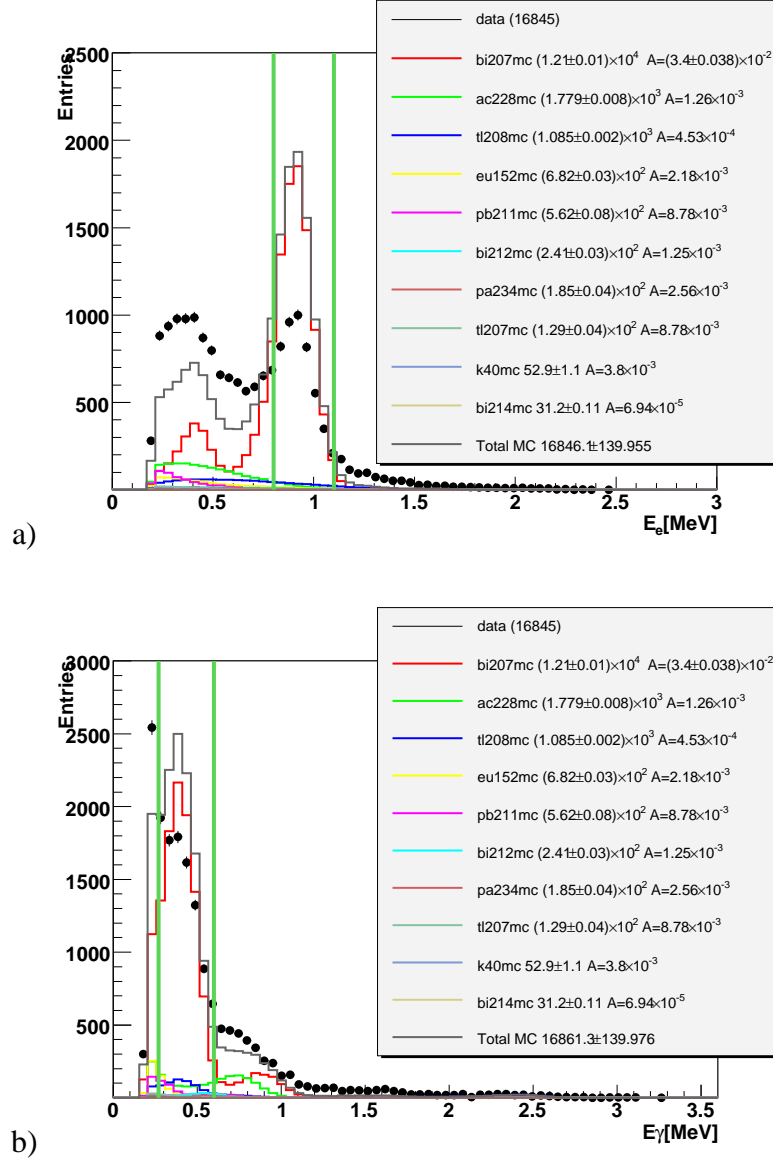
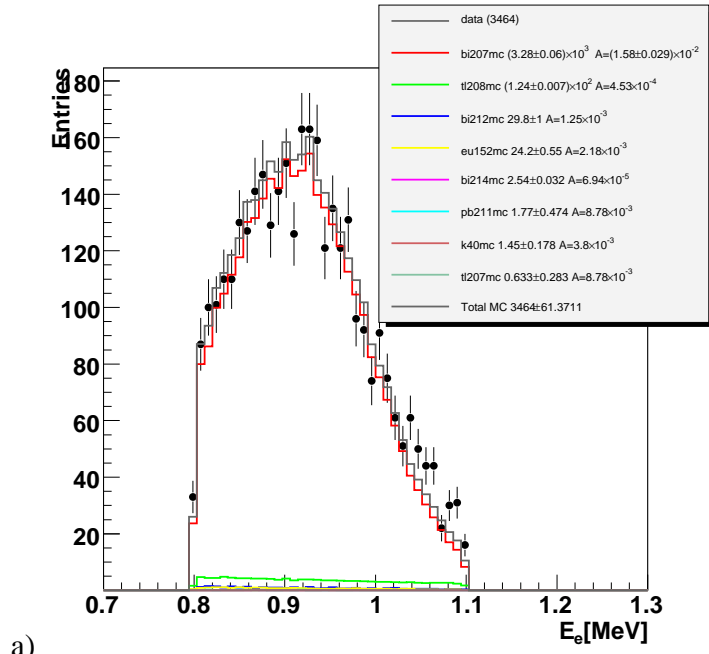
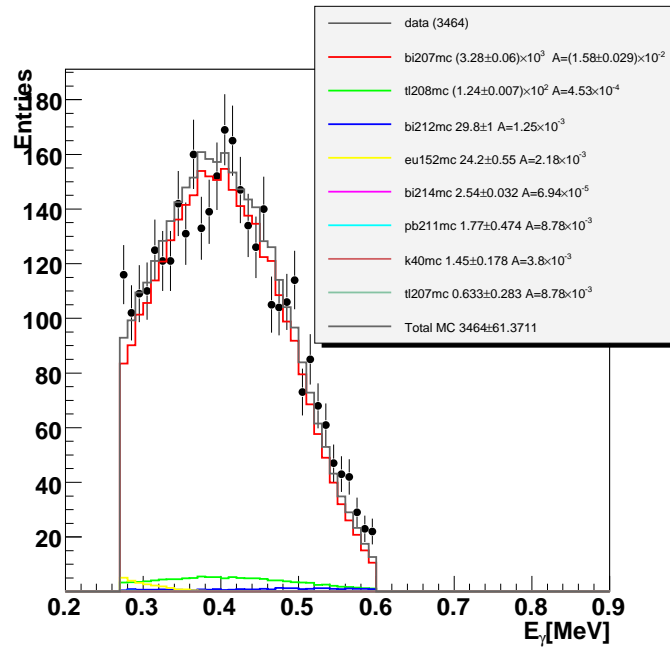


Figure 4.5: a) Distribution of the energy of the electron and b) Distribution of the energy of the γ -ray for $e\gamma$ channel. The number of simulated $2\nu\beta\beta$ events is scaled with the number of data minus background events. The data does not have a good fit with simulated events. Cuts are made in the energy region $0.8 < E_e < 1.1$ and $0.27 < E_\gamma < 0.6$, where the background is small.



a)



b)

Figure 4.6: a) Distribution of the energy of the electron and b) Distribution of the energy of the γ -ray for $e\gamma$ channel after applying $0.8 < E_e < 1.1$ and $0.27 < E_\gamma < 0.6$ energy conditions.

4.2.2 Other Sources of Background

There are other sources of internal background that need to be considered. The preliminary results of their activities are shown in table 4.1 [7]. These measurements are done with a Ge detector and are used previously in section 4.2.1. From Figure 4.5 it can be seen that they must be improved as part of this project.

To estimate the external background and the background coming from radon, the Cu foil in the detector is used. The double beta event selection criteria described in Section 4.1 are applied to events coming from Cu foil. The number of events left is 220 ± 15 and since Cu is not a double beta decay isotope, all these events are background to $2\nu\beta\beta$.

From MC simulation of Cu, it is found that 37% of the events come from radon and 51% of them come from external γ -ray background [8](other 12% of the events come from internal background). Therefore, about 81 ± 5 events come from radon and 112 ± 8 events come from external γ -ray source. These events are found for Cu foil and need to be scaled for Nd_2O_3 . The neodymium foil has only one strip compare to copper which has seven strips. This gives 12 ± 1 radon contaminant events. Neodymium and copper have different atomic numbers and therefore different electron density. The external γ -ray background to Nd_2O_3 needs to be rescaled by the ratio of their electron density:

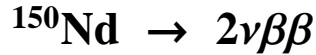
Isotope	^{208}Tl	$^{214}\text{Bi}, ^{214}\text{Pb}$	^{40}K	^{234m}Pa	$^{211}\text{Pb}, ^{207}\text{Tl}$	^{152}Eu	$^{228}\text{Ac}, ^{212}\text{Bi}$
Activity (mBq/kg)	7.95	1.217	66.7	45.0	154	38.3	22.1

Table 4.1: Contaminants of ^{150}Nd and a preliminary measurement of their activities in mBq/kg [7] done with the Ge detector.

$$R = \frac{\left(\frac{Z(Nd)}{A(Nd)\rho(Nd)d_{Nd}} + \frac{Z(O)}{A(O)\rho(O)d(O)}\right)^2}{\left(\frac{Z(Cu)}{A(Cu)\rho(Cu)d(Cu)}\right)^2} = \frac{1}{15}, \quad (4.5)$$

where Z is the atomic number, A is the atomic mass, ρ is the density, and d is the source foil thickness. From this ratio the number of external background events is found to be 7.5 ± 0.5 . Therefore, 19 ± 1 (stat) events are estimated to come from radon contaminant and external γ -ray.

4.3 Preliminary measurement of the half-life of



The number of expected events, derived from the radioactivity decay law and including the efficiency ϵ of the considered channel can be expressed by the following formula:

$$N(t) = \epsilon N_{at} (1 - e^{-\ln 2(t/T_{1/2})}), \quad (4.6)$$

where N_{at} is the number of atoms in a sample ($N_{at} = 1.48 \times 10^{23}$ for 37 gr of ^{150}Nd), t is the net data acquisition time, and $T_{1/2}$ is the half-life of the studied decay mode. Because of the large value of $T_{1/2}$ for $\beta\beta$ decays compared to t , one can rewrite equation 4.6 in the following way:

$$T_{1/2} = \epsilon N_{at} \ln 2 \frac{t}{N(t)} = \epsilon N_{at} \ln 2 \frac{t}{N_{exp} - N_{bgr}^{tot}}. \quad (4.7)$$

where N_{exp} is the number of experimental data events, and N_{bgr}^{tot} is the number of total background events.

By substituting the values presented in Table 4.3 in equation 4.7, the preliminary

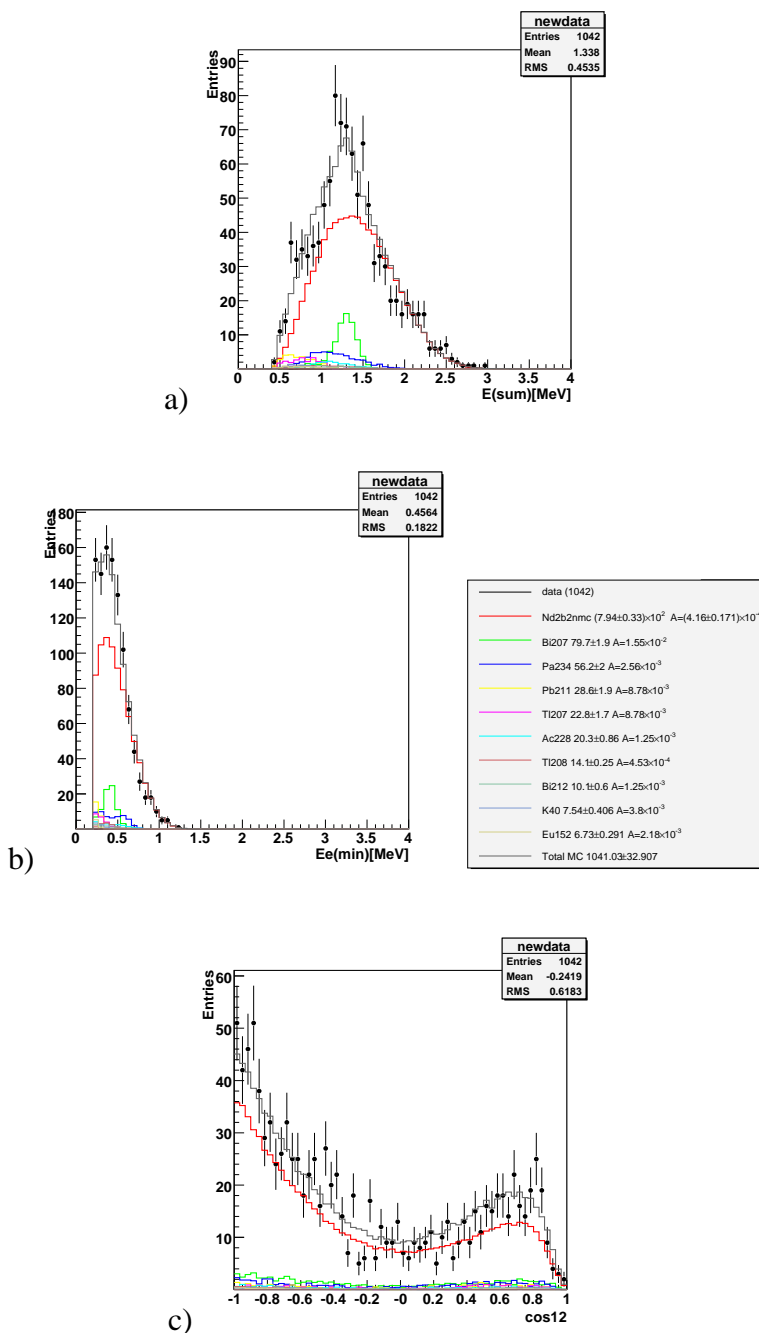


Figure 4.7: a) The sum of the energy of two electrons. b) The energy distribution of the lower energy electron. c) The cosine of the angle between two electrons. The $2\nu\beta\beta$ MC events are scaled with the number of data events minus the number of total internal background events.

Quantity	Fractional uncertainty	Value
$\epsilon_{2\nu\beta\beta}$	0.05 (syst)	$(6.6 \pm 0.3)\%$
N_{exp}	0.031 (stat)	1042 ± 32
$N_{207\text{Bi}}$	0.091 (syst)	80 ± 7
$N_{234m\text{Pa}}$	0.028 (syst)	56 ± 2
$N_{211\text{Pb}}$	0.05 (syst)	29 ± 1
$N_{207\text{Tl}}$	The Same	23 ± 1
$N_{208\text{Tl}}$	0.13 (syst)	14 ± 2
$N_{228\text{AC}}$	0.36 (syst)	20 ± 7
$N_{212\text{Bi}}$	0.36 (syst)	10 ± 4
$N_{40\text{K}}$	0.71 (syst)	7 ± 5
$N_{152\text{Eu}}$		7
$N_{214\text{Bi}}$		1
$N_{214\text{Pb}}$		0
N_{ext}	0.21 (stat)	19 ± 1
N_{bgr}^{total}	0.046	266 ± 12

Table 4.2: The table of results

result for $T_{1/2}$ is found to be:

$$T_{1/2} = (8.02 \pm 0.32 \text{ (stat)} \pm 0.41 \text{ (syst)}) \times 10^{18} \text{ years}, \quad (4.8)$$

where the systematic uncertainty comes from the systematic uncertainties on the efficiency and the activities. Figure 4.7 shows the distribution of the sum of the energy of two electrons, the energy of the electron with lower energy and the cosine of angle between electron tracks after correction on ^{207}Bi activity. The sum of the all MC events ($2\nu\beta\beta$ and background events) describes the experimental data with good precision. The result will be improved by doing the precise measurement of the activities of the other isotopes.

Chapter 5

Summary and Future Work

An internal background studies for $^{150}\text{Nd} \rightarrow 2\nu\beta\beta$ decays was presented in this report. The activity of ^{207}Bi was found to be

$$A = 272 + 21 \text{ (bgr)} \pm 14 \text{ (eff)} \pm 5 \text{ (stat)} \text{ mBq/kg}$$

and the preliminary value of the half-life of $^{150}\text{Nd} \rightarrow 2\nu\beta\beta$ was found to be

$$T_{1/2} = (8.02 \pm 0.32 \text{ (stat)} \pm 0.41 \text{ (syst)}) \times 10^{18} \text{ years}$$

by using this activity and other estimated contaminants activities.

To minimize the systematic uncertainty on background, this work continues with accurate measurement of ^{234}Pa , ^{207}Tl and ^{211}Pb activities by looking at the one-electron channel. Also the external background has to be studied by looking at the $e\gamma$ channel. Finally, after finding the precise value for the $2\nu\beta\beta$ half-life and measuring the final energy spectrum of the two electrons, the lower limit for the $0\nu\beta\beta$ half-life has to be found.

Bibliography

- [1] S. Eidelman et al., Phys. Lett. B 592,1 (2004).
- [2] P.W. Higgs, Spontaneous Symmetry Breakdown Without Massless Bosons, Phys. Rev. 145 (1966) 1156.
- [3] M. Goepfert, Phys. Rev. 48 (1935) 512
- [4] E. Majorana, Nuovo cimento 14 (1937) 171
- [5] M. Doi, T. Kotani and E. Takasugi, Phys. Rev. D 37 (1988) 2575.
- [6] Ruben Saakyan, Private Communication.
- [7] R. Arnold et al, Technical performance of the NEMO3 detector "Advantages and Limitation", NEMO3 internal note LAL 05-162 (November 2005).
- [8] Vladimir Vasiliev, Private Communication.

Acknowledgments

I would like to thank my supervisor Stefan Söldner-Rembold for his advice inspiration, encouragement and patience. I would also like to thank Vladimir Vasiliev of UCL for providing answers to my numerous questions and helping me to start this analysis. Finally, thanks to all the particle physics group in Manchester for helpful hints along the way and the School of Physics and Astronomy for my funding.